GEOPHYSICAL RESEARCH LETTERS, VOL. 35, L19310, doi:10.1029/2008GL035198, 2008

Next generation of deformation models for the 2004 M9 Sumatra-Andaman earthquake

Timothy Masterlark[1] and Kristin L. H. Hughes[1]

Received 1 July 2008; revised 5 September 2008; accepted 11 September 2008; published 14 October 2008.

[1] The 2004 M9 Sumatra-Andaman Earthquake (SAE) ruptured the interface separating the subducting Indo-Australian plate from the overriding Burma plate. We construct finite element models (FEMs) that simulate deformation of the earthquake for a three-dimensional problem domain partitioned to account for the distribution of material properties of the subducting slab, forearc, volcanic arc, and backarc. We demonstrate a protocol-based approach for simulating coseismic deformation, in which FEMs are implemented in inverse models to estimate the fault-slip distribution of the SAE while simultaneously honoring the geologic complexity of the subduction zone. Results suggest that deformation prediction sensitivities attributed to neglecting the different material properties of the subduction zone can be more than an order of magnitude greater than reported uncertainties for near-field GPS measurements. The FEM-based techniques presented here allow for geologically satisfying deformation models that will advance the reliability of modeling-based assessments of coseismic and postseismic deformation, stress-coupling, and tsunami genesis. **Citation:** Masterlark, T., and K. L. H. Hughes (2008), Next generation of deformation models for the 2004 M9 Sumatra-Andaman earthquake, *Geophys. Res. Lett.*, *35*, L19310, doi:10.1029/2008GL035198.

1. Introduction

[2] The 2004 M9 Sumatra-Andaman Earthquake (SAE) ruptured a 1200-km-long and 200-km-wide portion of the boundary separating the subducting Indo-Australian Plate from the overriding Burma Plate (Figure 1) [*Ammon et al.*, 2005; *Stein and Okal*, 2005]. The near-field deformation is characterized by 34 GPS sites that span the forearc and volcanic islands parallel to the Sunda trench (auxiliary material[1]). The combined magnitude and spatial extent of the observed SAE deformation provides exceptional opportunities to quantitatively simulate earthquake deformation. A generally overlooked, but significant distortion of simulation predictions is tied to the validity of deformation modeling techniques.

[3] Models provide the linkage between the observed surface deformation and the source of the deformation – the fault-slip at depth. While forward models allow us to predict deformation caused by fault-slip, substantial effort has gone into the development of inverse models that strive to quantify fault-slip, based on observed deformation and a priori forward deformation models. In practice, relatively little attention is given to the implications of the a priori forward models and sensitivity analyses of deformation model assumptions are rare [*Masterlark*, 2003]. A suitable deformation model, which includes a self-consistent fault-slip distribution, is the key to any analysis of coseismic deformation, tsunami-genesis, postseismic deformation, or stress-coupling [*Freed et al.*, 2006; *Masterlark*, 2003; *Sobolev et al.*, 2007]. The reliability of SAE deformation interpretations is contingent on three fundamental elements: the quantity and quality of the deformation data, the suitability of the inverse scheme, and the validity of the deformation model, the latter of which is the focus of this study.

[4] The cold, downgoing slab is the essence of a subduction zone and its relative stiffness significantly impacts deformation predictions for megathrust earthquakes [*Masterlark*, 2003]. Deformation models for dislocations in homogeneous elastic half-spaces (HEHS) [e.g., *Okada*, 1992] are overwhelmingly implemented to describe, assess, and interpret observed deformation of the SAE [*Han et al.*, 2006; *Nalbant et al.*, 2005; *Vigny et al.*, 2005]. Alternatively, models that simulate horizontally layered elastic half-spaces (LEHS) are implemented to simulate an assumed layered structure of the Earth [*Chlieh et al.*, 2007; *Subarya et al.*, 2006]. Both of these models ignore the known presence, geometric complexity, and significance of the relatively stiff subducting slab.

[5] FEMs permit us to simulate variable slip along fault surfaces embedded in a problem domain that accounts for the juxtaposition of the stiff, dipping subducting slab and relatively compliant overriding plate, as well as the material property variations of the forearc, volcanic arc, and backarc regions. Furthermore, FEMs are readily implemented in linear inverse analyses of observed deformation due to the fault-slip of an earthquake [*Masterlark*, 2003; *Schmitt et al.*, 2007]. In spite of these known capabilities, FEMs are rarely invoked for inverse analyses of static earthquake deformation. We provide methods to replace standard HEHS and LEHS models that are computationally efficient, but poorly represent the geologic complexity of the subduction zone, with computationally intensive FEMs that can readily provide geologically satisfying configurations for the SAE. The inability to reliably predict recent events triggered by the SAE fault-slip reflects the need to pursue better deformation models. The integration of geology into deformation modeling methods is a critical and necessary advancement toward more reliable predictions and early warning systems for earthquake stress-coupling [*Masterlark*, 2003] and tsunami-genesis [*McCloskey et al.*, 2008].

[1]Department of Geological Sciences, University of Alabama, Tuscaloosa, Alabama, USA.

0094-8276/08/2008GL035198$05.00

[1]Auxiliary materials are available in the HTML. doi:10.1029/2008GL035198.

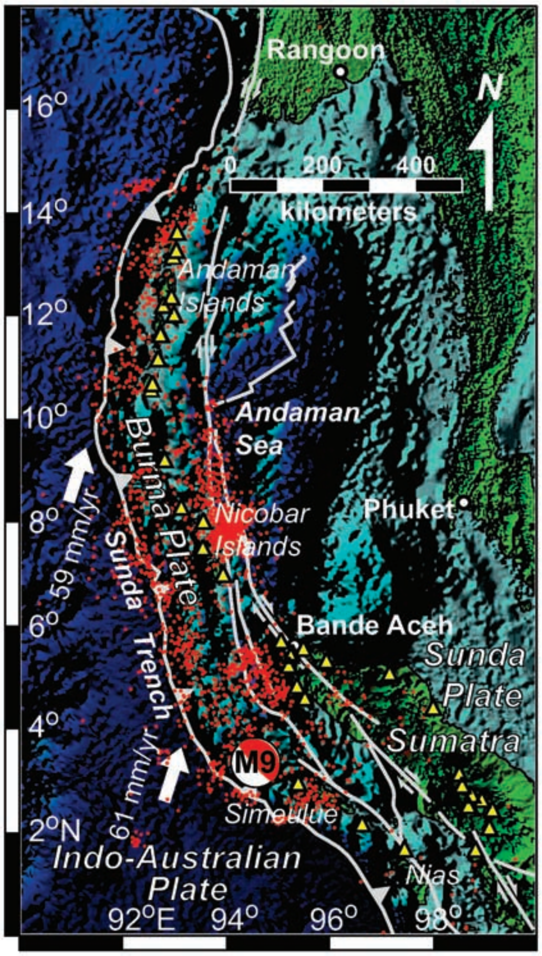

Figure 1. Seismotectonic setting. The Havard CMT focal mechanism overlies the epicenter of the SAE. Aftershock epicenters (red dots) illuminate the surface projection of the rupture (http://neic.usgs.gov), which initiated on the southeast portion of the fault and propagated 1200 km northward. Yellow triangles are near-field GPS sites, summarized in Table S1. The tectonic configuration is modified from *Bird* [2003] and overlies a shaded relief image of global relief data (http://www.ngdc.noaa.gov).

[6] The remainder of this paper is organized into three sections. First, the main body introduces the FEM-based deformation modeling protocol and describes its implementation for the SAE. We present a fault-slip distribution for the SAE that is calibrated to GPS data for a deformation model that honors the know structure of the subduction zone. We then present a discussion of the results and implications of the protocol-based modeling and how the predictions differ from those of standard deformation models. This discussion includes several possibilities for improving the model through reassessment, a concept that is central to protocol-based modeling. Finally, we present conclusions and recommendations.

2. Deformation Modeling Protocol

[7] Inspired by the formal protocol that standardizes groundwater modeling analyses [*Anderson and Woessner*, 1992], we introduce a deformation modeling protocol to guide and test the model design and ensure the deformation model adequately represents the natural system (Figure 2a). FEM-based techniques are embedded in the modeling protocol and allow us to estimate the fault-slip distribution and predict near-field deformation, while simultaneously honoring the known geologic complexity associated with the SAE. This protocol calls for reassessment at any stage, in which the model either fails to adequately represent the known problem domain constraints or effectively predict observations. This call for reassessment and ability to implement improvements in deformation model configurations via FEMs is a significant departure from standard HEHS-based analyses, for which the fault geometry and slip are the only permissible variations.

[8] The design of the conceptual model is the foundation of the deformation modeling protocol and therefore a fundamental consideration for predicting earthquake deformation. Implications of the conceptual model propagate throughout the modeling analysis and shape predictions and interpretations. Our conceptual model of the SAE relates near-field coseismic deformation to the fault-slip distribution as the mechanical response of a three-dimensional elastic/poroelastic problem domain to an embedded dislocation. The deformation is static and undrained, that is, the deformation that remains after dynamic wave propagation, but prior to postseismic fluid flow in the brittle crust and viscoelastic flow of the mantle. A representative cross-section of the subduction zone is constructed as an 800-km-long trench-normal slice through the Sumatra region (Figure 2b). Seismicity data [*Engdahl et al.*, 2007] constrain the geometry of the subducting slab. The fault-slip of the SAE occurs along the interface separating the subducting slab, consisting of lithospheric mantle capped by mid-oceanic ridge basalt, and the overriding forearc and upper mantle wedge [*Kieckhefer et al.*, 1980; *Kopp and Kukowski*, 2003; *Kopp et al.*, 2002]. Geologic maps and cross-sections of Sumatra [*Barber et al.*, 2005; *Kopp and Kukowski*, 2003; *Kopp et al.*, 2002] guide the configuration of the volcanic arc and backarc basin of the overriding plate. This two-dimensional cross section is swept through the curving strike of the Sunda trench from northern Sumatra through the Andaman Islands to produce a three-dimensional model (Figure 2c). A limitation of this configuration is the constant cross-section along the trench, which does not account for along-strike variations associated with the transition of island arc volcanism in Sumatra to the back-arc spreading in the Andaman Basin (Figure 1) [*Curray*, 2005]. This additional complexity will be addressed in future modifications to the model configuration.

[9] All FEMs in this study are constructed with Abaqus (http://www.simulia.com) and solve the elastic and poroelastic governing equations [*Wang*, 2000] over the three-dimensional problem domain. The free surface at the top of the problem domain represents the Earth's surface. The top of the simulated oceanic crust represents a flat seafloor having a reference elevation of zero. The free-surface along the toe of the thrust includes a transition from the seafloor to the top surface of the overriding continental plate, which has a simulated reference elevation of 4 km. More detailed relief significantly affects neither deformation predictions nor fault-slip estimations [*Masterlark*, 2003]. The lateral boundaries and base of

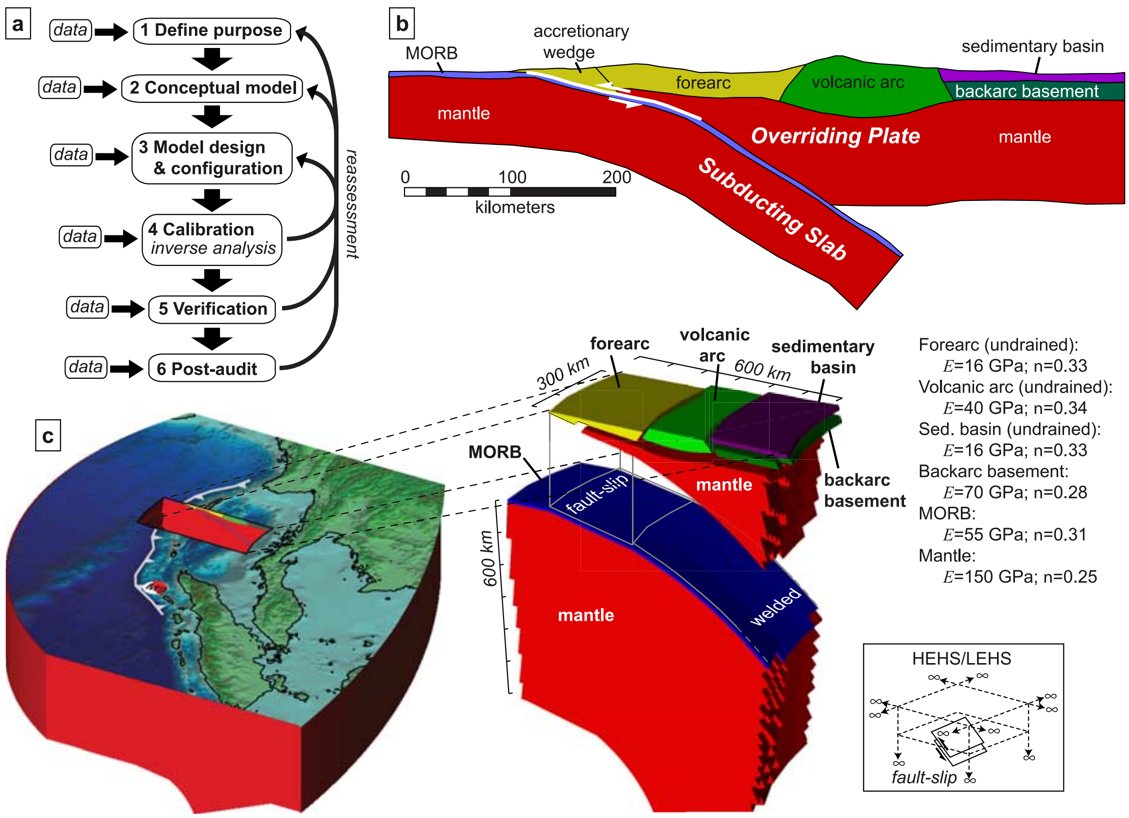

Figure 2. Protocol-based deformation model for the SAE. (a) Protocol. The protocol ensures that the modeling progression honors the available information and provides a mechanism for iterative reassessment. (b) Conceptual model. This design includes geologic constraints discussed in the text. (c) FEM design and configuration. The FEM comprises about 340,000 elements. The exploded view reveals the likeness of the FEM to the geologic structure of the conceptual model. Neither the HEHS nor the LEHS configuration (bottom right) accounts for the relatively stiff subducting slab and associated structures shown in the conceptual model.

the problem domain have zero displacement. We simulate fault-slip by imposing kinematic constraint equations [*Masterlark*, 2003] for 165 fault-patches along the curving rupture interface (auxiliary material). The converging plates are welded together along the non-slipping portions of the plate boundary. The initial conditions are equilibrium, therefore deformation, stress, and pore pressure predictions are incremental changes with respect to the state of the system prior to the fault-slip. Material properties are taken from compilations of elastic [*Turcotte and Schubert*, 1982] and poroelastic [*Wang*, 2000] rock properties. The FEM validation for using kinematic constraint equations to simulate elastic dislocations is described in the auxiliary material.

[10] For a system of multiple displacement observations and a distribution of fault-slip patches along the rupture, the net displacement for a given GPS site is the superposition of contributions from each fault-patch. Green's functions for displacement are calculated by predicting displacement caused by unit slip over a given fault-patch while simultaneously welding the remaining fault-patches. We implement an algorithm that systematically generates the unit slip and welding configuration over the rupture, executes the model, and extracts the Green's functions for both thrust and strike-slip components for each fault-patch. We invert the resulting system of linear equations to estimate the distribution of fault-slip (auxiliary material). Results suggest that more than 20 meters of fault-slip occurred along the southern two-thirds of the rupture (Figure 3a). This band of slip is generally deeper along the southern end of the rupture and becomes shallower to the north. The thrust component dominates along the entire rupture. The right-lateral strike-slip component is minimal along the southern end and increases northward. This calibrated FEM, loaded by this fault-slip distribution, adequately predicts the observed GPS deformation (Figure 3).

3. Discussion

[11] We modify the FEM to simulate an HEHS to test the sensitivity of deformation predictions to the distribution of material properties. Green's functions are calculated and assembled for this HEHS and a fault-slip distribution is estimated with the same inverse scheme. The general magnitude of the estimated fault-slip distribution for the HEHS is somewhat reduced compared to that of the heterogeneous FEM (Figure 3b). The differences are most pronounced west of Northern Sumatra and GPS displacement sensitivities to the distribution of material properties are significantly greater than GPS measurement uncertain-

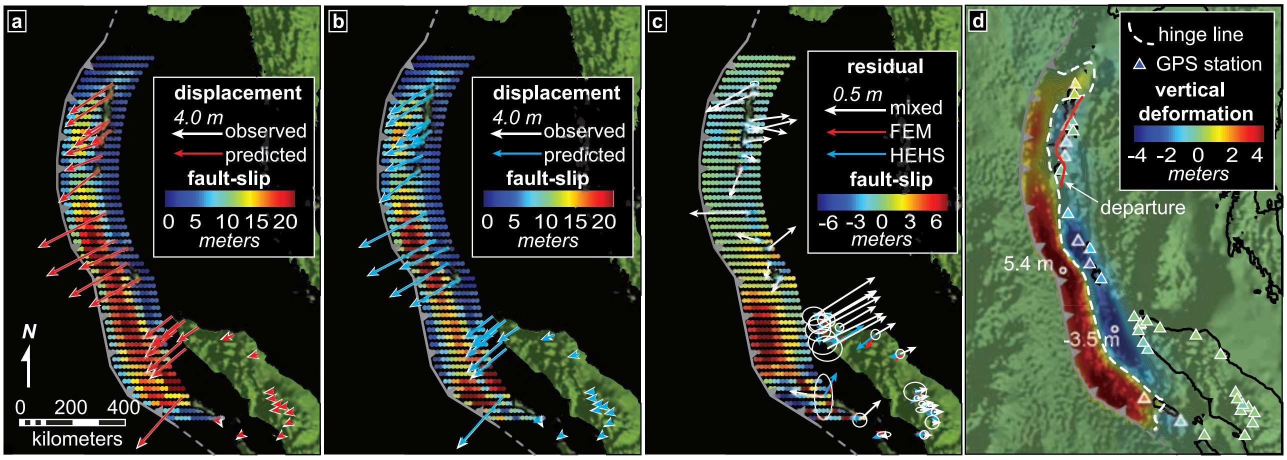

Figure 3. Calibration. (a) FEM. (b) HEHS. (c) Model-dependent prediction errors. The model-dependent sensitivity of displacement predictions is illustrated by loading the FEM with the difference between the estimated FEM and HEHS slip distributions. This sensitivity is significantly greater than GPS measurement uncertainties, shown as 1σ ellipses. The fault-slip distribution shown here is the difference between fault-slip distributions estimated for the FEM and HEHS models. (d) Coseismic vertical deformation, FEM. White circles correspond to locations of predicted vertical displacement extremes.

ties (Figure 3c). In spite the differing estimated fault-slip distributions, both the FEM and HEHS models predict the GPS deformation equally well, as shown by the residual in Figure 3c and discussed in the auxiliary material. Although both models can predict the observed coseismic deformation data, forward model predictions for tsunami genesis and stress-coupling processes that are driven by the differing estimated fault-slip distribution may vary significantly, due to the magnitude and spatial extent of the fault-slip differences [*Masterlark*, 2003; *McCloskey et al.*, 2008; *Sobolev et al.*, 2007]. Thus, the validity of a given SAE deformation model configuration will influence the associated interpretations of forward model predictions.

[12] The verification step is an assessment of the model's predictive reliability. In this step, we test if the model successfully predicts data that are independent of the calibration process. Coral measurements and optical remote sensing observations characterize the vertical deformation pattern of the SAE along a sinuous, trench-parallel trajectory [*Meltzner et al.*, 2006]. Vertical deformation predictions from the calibrated FEM generally agree with these data (Figure 3d). The minor departure of our predicted axis of zero vertical deformation separating the near-field uplift and subsidence near the Andaman Islands may be a result of the constant trench-normal cross-section configuration of the FEM. Future work will investigate alternative model configurations that account for the along-strike variations in geometry and material properties.

[13] The predicted vertical deformation substantially underestimates the seafloor uplift near the trench that is required for models of tsunami genesis [*Geist et al.*, 2007; *Ioualalen et al.*, 2007]. One way to resolve this problem is to increase the seafloor uplift by imposing a penalty function that favors shallow fault-slip in the inverse analysis [*Menke*, 1989]. However, there is no obvious physical basis for this ad-hoc constraint that would be at odds with seismologic data [*Ammon et al.*, 2005]. Alternatively, we can approach this discrepancy by revising the conceptual model to include splay faults in the toe of the thrust [*Kopp and Kukowski*, 2003] or a partitioning of the forearc into a more refined distribution of stiff and compliant regions, such that the fit to the GPS data is optimized while simultaneously increasing the near-trench uplift. Both of these configurations are supported by geologic and geophysical data [*Fisher et al.*, 2007; *Kieckhefer et al.*, 1980; *Kopp et al.*, 2002]. This reassessment of the conceptual model design is another avenue toward future improvements of the model configuration.

[14] The real power of FEM-based analyses lies in their ability to predict not only the coseismic deformation of the earthquake, but to simulate multiple postseismic deformation processes that are driven by fault-slip. We entered the protocol with the purpose of simulating the coseismic deformation of the SAE. Consequently, the FEM is calibrated and verified for the static coseismic deformation of the SAE and was not designed to simulate the ongoing postseismic deformation that is observed with GPS data [*Chlieh et al.*, 2007]. Because of this additional information, the protocol requires a reassessment of our fundamental purpose, which will address postseismic processes that are driven by the coseismic fault-slip. This reassessment is within the domain of the protocol and FEM capabilities and yet another direction for future improvements of SAE deformation models. The FEM-based protocol treats deformation modeling as a dynamic process that is continuously subject to iterative improvements in an effort to better simulate the natural deformational system and ultimately provide reliable deformation predictions.

4. Conclusions

[15] We demonstrate an approach, in which geologically satisfying FEMs are implemented in both forward and inverse models of coseismic deformation for the SAE. The FEM-based techniques, embedded in the modeling protocol, provide powerful tools to explore various aspects

of coseismic fault-slip, while simultaneously honoring the rich geologic complexity associated with a subduction zone. The call for reassessment and the ability to explicitly modify deformation model configurations accordingly, is a fundamental advancement in assessments of earthquake deformation. Estimations of the fault-slip distribution and near-field deformation for the SAE, based on HEHS and LEHS model predictions, are significantly distorted, a result that propagates into interpretations of SAE deformation. The methods presented here can rectify these distortions and lead to more accurate interpretations and inferences in future modeling-based assessments of coseismic deformation, postseismic deformation, stress-coupling, and tsunami genesis.

[16] **Acknowledgments.** This work is supported by NASA under award NNX06AF10G. Academic licensing for Abaqus software is provided by Simulia, Dassault Systèmes.

References

Ammon, C. J., et al. (2005), Rupture process of the 2004 Sumatra-Andaman Earthquake, *Science*, *308*, 1133–1139.

Anderson, M. P., and W. W. Woessner (1992), *Applied Groundwater Modeling: Simulation of Flow and Advective Transport*, 381 pp., Academic, San Diego, Calif.

Barber, A. J., M. J. Crow, and J. S. Milsom (2005), *Sumatra: Geology, Resources, and Tectonic Evolution*, 290 pp., Geol. Soc., London.

Bird, P. (2003), An updated digital model of plate boundaries, *Geochem. Geophys. Geosyst.*, *4*(3), 1027, doi:10.1029/2001GC000252.

Chlieh, M., et al. (2007), Coseismic slip and afterslip of the great M_w 9.15 Sumatra-Andaman earthquake of 2004, *Bull. Seismol. Soc. Am.*, *97*, S152–S173.

Curray, J. R. (2005), Tectonics and history of the Andaman Sea Region, *J. Asian Earth Sci.*, *25*, 187–232.

Engdahl, E. R., A. Villaseñor, H. R. DeShon, and C. H. Thurber (2007), Teleseismic relocation and assessment of seismicity (1918–2005) in the region of the 2004 M_w 9.0 Sumatra-Andaman and 2005 M_w 8.6 Nias Island great earthquakes, *Bull. Seismol. Soc. Am.*, *97*, S43–S61.

Fisher, D., D. Mosher, J. A. Austin Jr., S. P. S. Gulick, T. Masterlark, and K. Moran (2007), Active deformation across the Sumatran forearc over the December 2004 M_w 9.2 rupture, *Geology*, *35*, 99–102.

Freed, A. M., R. Bürgmann, E. Calais, J. Freymueller, and S. Hreinsdóttir (2006), Implications of deformation following the 2002 Denali, Alaska, earthquake for postseismic relaxation processes and lithospheric rheology, *J. Geophys. Res.*, *111*, B01401, doi:10.1029/2005JB003894.

Geist, E. L., V. V. Titov, D. Arcas, F. F. Pollitz, and S. L. Bilek (2007), Implications of the 26 December 2004 Sumatra-Andaman earthquake of tsunami forecast and assessment models for great subduction-zone earthquakes, *Bull. Seismol. Soc. Am.*, *97*, S249–S270.

Han, S.-C., C. K. Shum, M. Bevis, C. Ji, and C.-Y. Kuo (2006), Crustal dilatation observed by GRACE after the 2004 Sumatra-Andaman earthquake, *Science*, *313*, 658–662.

Ioualalen, M., J. Asavanant, N. Kaewbanjak, S. T. Grilli, J. T. Kirby, and P. Watts (2007), Modeling the 26 December 2004 Indian Ocean tsunami: Case study of impact in Thailand, *J. Geophys. Res.*, *112*, C07024, doi:10.1029/2006JC003850.

Kieckhefer, R. M., G. G. Shor Jr., J. R. Curray, W. Sugiarta, and F. Hehuwat (1980), Seismic refraction studies of the Sunda trench and forearc basin, *J. Geophys. Res.*, *85*, 863–889.

Kopp, H., and N. Kukowski (2003), Backstop geometry and accretionary mechanics of the Sunda margin, *Tectonics*, *22*(6), 1072, doi:10.1029/2002TC001420.

Kopp, H., D. Klaeschen, E. R. Flueh, J. Bialas, and C. Reichert (2002), Crustal structure of the Java margin from seismic wide-angle and multichannel reflection data, *J. Geophys. Res.*, *107*(B2), 2034, doi:10.1029/2000JB000095.

Masterlark, T. (2003), Finite element model predictions of static deformation from dislocation sources in a subduction zone: Sensitivities to homogeneous, isotropic, Poisson-solid, and half-space assumptions, *J. Geophys. Res.*, *108*(B11), 2540, doi:10.1029/2002JB002296.

McCloskey, J., A. Antonioli, A. Piatanesi, K. Sieh, S. Steacy, S. Nalbant, M. Cocco, C. Giunchi, J. Huang, and P. Dunlop (2008), Tsunami threat in the Indian Ocean from a future megathrust earthquake west of Sumatra, *Earth Planet. Sci. Lett.*, *265*, 61–81, doi:10.1016/j.epsl.2007.09.034.

Meltzner, A. J., K. Sieh, M. Abrams, D. C. Agnew, K. W. Hudnut, J.-P. Avouac, and D. H. Natawidjaja (2006), Uplift and subsidence associated with the great Aceh-Andaman earthquake of 2004, *J. Geophys. Res.*, *111*, B02407, doi:10.1029/2005JB003891.

Menke, W., (1989), *Geophysical Data Analysis: Discrete Inverse Theory*, *Int. Geophys. Ser.*, vol. 45, 289 pp., Academic, San Diego, Calif.

Nalbant, S. S., S. Steacy, K. Sieh, D. Natawidjaja, and J. McCloskey (2005), Earthquake risk on the Sunda trench, *Nature*, *435*, 756–757.

Okada, Y. (1992), Internal deformation due to shear and tensile faults in a half-space, *Bull. Seismol. Soc. Am.*, *82*, 1018–1040.

Schmitt, S. V., C. DeMets, J. Stock, O. Sánchez, B. Márquez-Azúa, and G. Reyes (2007), A geodetic study of the 2003 January 22 Tecomán, Colima, Mexico earthquake, *Geophys. J. Int.*, *169*, 389–406, doi:10.1111/j.1365-246X.2006.03322.x.

Sobolev, S. V., A. Y. Babeyko, R. Wang, A. Hoechner, R. Galas, M. Rothacher, D. V. Sein, J. Schröter, J. Lauterjung, and C. Subarya (2007), Tsunami early warning using GPS-Shield arrays, *J. Geophys. Res.*, *112*, B08415, doi:10.1029/2006JB004640.

Stein, S., and E. A. Okal (2005), Speed and size of the Sumatra earthquake, *Nature*, *434*, 581–582.

Subarya, C., M. Chlieh, L. Prawirodirdjo, J.-P. Avouac, Y. Bock, K. Sieh, A. J. Meltzner, D. H. Natawidjaja, and R. McCaffrey (2006), Plate-boundary deformation associated with the great Sumatra-Andaman earthquake, *Nature*, *440*, 46–51.

Turcotte, D. L., and G. J. Schubert (1982), *Geodynamics: Applications of Continuum Physics to Geological Problems*, 450 pp., John Wiley, New York.

Vigny, C., et al. (2005), Insight into the 2004 Sumatra-Andaman earthquake from GPS measurements in Southeast Asia, *Nature*, *436*, 201–206.

Wang, H. F. (2000), *Theory of Linear Poroelasticity: With Applications to Geomechanics*, 287 pp., Princeton Univ. Press, Princeton, N. J.

K. L. H. Hughes and T. Masterlark, Department of Geological Sciences, University of Alabama, Tuscaloosa, AL 35487, USA. (masterlark@geo.ua.edu)